A set-theoretic approach to analyzing timing uncertainty within cyber-physical systems

D.M. Anand, *National Institute of Standards and Technology*
Gaithersburg, MD 20899

BIOGRAPHY (IES)

D. M. Anand is a Research Scientist with the National Institute of Standards and Technology. His research interests include the dynamics, control, fault diagnosis and optimization of distributed networked systems. Application domains of particular interest include power systems, industrial control systems and cyber-physical systems where humans participate cognitively.

ABSTRACT

Clocks are deeply integrated into practically every cyber-physical system either explicitly as provenance for time-triggered actions, or implicitly in cases where cyber components operate in lock step with physical dynamics. Recognizing the criticality of timing components, this paper investigates an analysis approach that allows a system designer to formally incorporate timing uncertainty as a factor when evaluating the uncertainty of the overall cyber-physical system. A set theoretic approach is considered in this paper that offers advantages in the form of computational scalability and in its ability to accommodate a general class of hybrid dynamic systems. A demonstration of the approach is provided via illustrative example using a charge pump phase locked loop and a second order dynamic system. We anticipate that the proposed approach is particularly applicable to systems where safety or reachability guarantees are required.

1) INTRODUCTION

Unification and global traceability of time scales are particularly critical in systems spread over a wide geographical area where collaborative actions between components are frequently imputed to UTC. Examples of such systems include the cellular telecom network, the electric power system and wide area process control systems (pipelines and gas supply networks).

Most of these cyber-physical systems (CPS) involve controllers, consisting of: (a) a set of sensors and actuators, representing the interface between the controller and its environment; (b) a control logic (implemented as one or more circuits or as one or more pieces of software running concurrently); and (c) the underlying timing system, which determines the rate, precision and accuracy of coordinated actions. Such systems are commonly modeled as hybrid automata. Hybrid automata are finite-state machines equipped with continuous variables. Each discrete state of an automaton has a system of differential equations that govern its continuous variables.

When designing a CPS or while integrating components into a CPS, designers typically perform correctness tests of the system as a whole. These tests typically evaluate all likely behaviors or trajectories of the system against a set of 'performance' criteria [1]. A simplified notion of performance would be that the system provides the minimum expected functionality while not entering an unsafe or bad state. Ensuring correctness, however, is often not a trivial task. Simulation of the system is not adequate, since it can only help examine a limited number of trajectories. Analytical methods are often not applicable, considering the complexity of systems with a large number of dynamic interactions.

Analytical and simulation studies are particularly inadequate when assessing the safety of a closed-loop CPS in relation to uncertainty associated with timing components [2]. Firstly, the timing system is a CPS in itself, characterized by interacting continuous (Phase and Frequency Locking) and discrete (Synchronization logic) states. Further, the stochastic properties of oscillators are rarely amenable to closed form analytical expression. And lastly, manufacturer data for clocks frequently represent uncertainty in the form of bounded sets (min/max, PPM) making simulation studies impractical.

An alternative to analytical and simulation studies is reachability analysis [3]. It consists of computing the set of all reachable states of the system and then checking that an application specific safe set encloses it. In our paper we focus on analyzing the impact of timing uncertainty on safety criteria. Reachability, as used in our analysis, involves mapping the performance envelope for the timing system onto the safe set for an enclosing CPS.

In our paper we consider a timing subsystem comprised of a Type-II Charge Pump Phase Locked Loop (PLL) and model (as hybrid automata) the interactions between a VCO, a three state phase frequency detector, a loop filter and frequency divider.

In Section 2 we present the model of our system including the hybrid automata we use to describe it. In Sections 3 and 4 we introduce our geometric interpretation of uncertainty and apply it to sensor uncertainty and uncertainties associated with the PLL system respectively. Section 5 presents hybrid set theoretic reachability and the geometric results that enable our analysis. Finally, Section 6 concludes our analysis by highlighting some preliminary results showing that the correctness of a synchronous generator control system can be evaluated from the perspective of measurement uncertainty (combining sensor and timing uncertainty) using our set theoretic approach. We also propose next steps for the work presented in this paper.

2) HYBRID AUTOMATA

A linear hybrid automaton is a generalized finite state automaton that is equipped with continuous variables. The discrete changes of the hybrid system are modeled by edges of the automaton and the continuous evolution of the system at each location in the automaton is constrained by linear time invariant dynamics of the form $\dot{x} = Ax + Bu$. The syntax we use for hybrid automaton in our paper is defined in detail in [4].

Following conventional notation, let us consider a hybrid automaton H represented by the tuple $\langle Loc, Edge, \Sigma, X, Init, Flow, Jump \rangle$ where $Loc: \{l_1, l_2 \dots l_m\}$ is a set of finite control locations that represent control modes. Instantaneous discrete transitions between control modes are denoted with a set of labeled edges $Edge \subseteq \Sigma \times Loc$ where the labels are drawn from set Σ. The automaton is equipped with a set of differentiable continuous variables $X \in \mathbb{R}^n$, with $\dot{X}$ and $\acute{X}$ representing the first derivative and the updated value of X respectively. The $Init$ and Inv predicates attached to each location in the automaton represent inequality constraints on the initial value and magnitude limits of X within each mode respectively. Finally, the functions $Flow$ and $Jump$ represent the evolution trajectory acting on $X \cup \dot{X}$ and the discrete update acting on $X \cup \acute{X}$ respectively.

2.1) Running CPS example

To illustrate the analysis approach in this paper let us consider a simplified example of a control problem requiring synchronized clocks. The example we use in this paper is based on the control requirements for power regulation in a 'microgrid' [5]. Microgrids with multiple generators require precise coordination of generator set points in order to maintain stable voltage and frequency. This coordination is particularly critical in a small power grid that is susceptible to fluctuations in voltage magnitude and frequency due to changes in loads, or external conditions such as a fault on the main grid. Control methodologies must respond to local variations in voltage waveforms, while still tracking a reference performance schedule for the microgrid. Since microgrids can span several hundred meters in area, control and sensor signals are typically transmitted over an Ethernet network, with control authority delegated to multiple generators. Accurate clock synchronization is required across all generators, sensors and circuit breakers to ensure operation of the entire networked control system.

A simplified dynamic representation of the microgrid problem is shown in Figure 1. In our example, we assume two generators represented by the linearized swing dynamics as shown in Equation 1 coupled through a complex impedance Z_{12}. This simplified example highlights the coupling interaction between two sets of 2nd order differential equations. In the case of our example, the impedance between the generators manifests dynamics corresponding to a first order filter in the form of a phase lag between b_1 and b_2. The dynamic response of each generator is governed by its rotary inertia and damping ratio J_i and D_i respectively. The state of each generator is represented by its terminal voltage E_i and rotor angle δ_i. The generator is controlled via regulation of input power $P_{g,i}$. The cumulative dynamics of the two-generator system in response to perturbations of the state $[V_i, \theta_i]^T$ about a synchronized network in steady state may be represented by the dynamic linearized swing equation and the algebraic DC power flow equation. These equations can be assembled into a state-space model for the network, producing a small signal version of the structure-preserving power network model shown in Equation 2 as derived in [6].

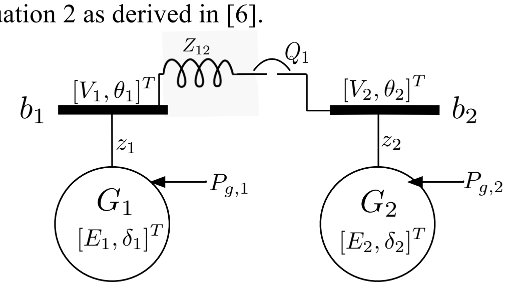

Figure 1: Schematic representation of a two generator microgrid

Equation 1: Linearized swing equation for generators

$$\dot{\delta}_i(t) = \omega_i(t),$$
$$J_i \dot{\omega}_i = P_{g,i}(t) - \frac{E_i V_i}{z_i}(\delta_i(t) - \theta_i(t)) - D_i \omega_i(t)$$

Equation 2: Structure preserving power network model

$$\begin{bmatrix} I & 0 & 0 \\ 0 & J & 0 \\ 0 & 0 & 0 \end{bmatrix} \begin{bmatrix} \dot{\delta}(t) \\ \dot{\omega}(t) \\ \dot{\theta}(t) \end{bmatrix} = - \begin{bmatrix} 0 & -I & 0 \\ L_{gg} & D & L_{gl} \\ L_{lg} & 0 & L_{ll} \end{bmatrix} \begin{bmatrix} \delta(t) \\ \omega(t) \\ \theta(t) \end{bmatrix} + \begin{bmatrix} 0_{(1:n)} \\ Pg_{(1:n)} \\ P_{(1:m)} \end{bmatrix}$$

Assuming that the generators in the network are of PV-Type [7], we can decouple Equation 2 into a system of Ordinary Differential Equations in the linear time invariant form $\dot{x} = Ax + Bu$ and a set of linear algebraic constraints $\alpha \geq [\mathbb{Z}_{12}]^{-1} x$ on the relative phase between adjacent buses where $[\mathbb{Z}_{12}]$ is the impedance weighted adjacency matrix for the two generator circuit. Note that such algebraic constraints are compatible with the Inv

predicate defined in Section 2. Let us now consider the discrete changes in the circuit topology represented by the circuit breaker Q_1. In the event of a large fault current between b_1 and b_2, the phase constraint represented by Z_{12} is released and the two generators operate independently. In power systems terms, this event represents a fault triggered decoupling event. Q_1 may be triggered by other considerations such as a phase angle, thermal or voltage excursions. In our formalism for hybrid automata these triggers comprise the $Jump$ predicate.

Without the loss of generality, we can reduce the microgrid regulation control problem within each operating mode of the circuit breaker to a phase synchronization problem for G_2. The synchronization torque for G_2 is given by the equation:

$$P_{g,2} = \frac{V_1 V_2}{Z_{12}} \cos(\theta_1 - \theta_2)$$

Integrating this control law into the dynamics in Equation 2 and linearizing the system we get a closed loop system of the form $\dot{x} = [A + BK]x$. The closed loop system after a circuit breaker tripping event is represented by $\dot{x} = [A^* + BK^*]x$. Combining both operating modes, we get the hybrid system shown in Figure 2.

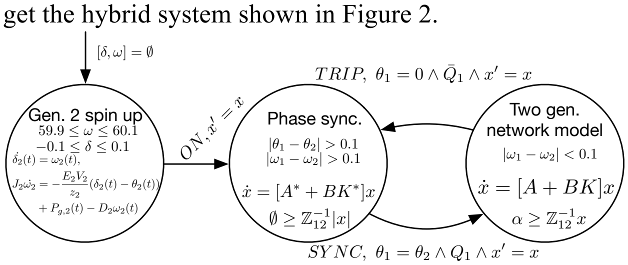

Figure 2: Hybrid automata describing the three operating modes for the two generator system.

3) SENSOR UNCERTAINTY

The sources of uncertainty that limit the performance of the phase tracking control problem range from model errors, to inaccuracies in measurements to actuator bandwidth limitations and network latency. Since Equation 1 has an inherent pole at the origin (an integrator), our generator phase synchronization problem presents a tracking error that is proportional to the integral of any error in the control inputs. The control input $P_{g,i}$ in turn, is an algebraic function of the system state with a gain proportional to Z_{12}^{-1}. For most distribution circuits, this gain is in the order of about 10^4 making the control system particularly sensitive to uncertainties in the system state x.

Inaccuracies in the estimation/measurement of the system state will be the primary focus of our analysis in this paper in keeping with growing interest in the microgrid community for real time, high quality sensor measurements. The state of our example system (Equation 2) includes the explicit variables $[\theta, \delta]$ that correspond to measurements of phase on circuit buses and generator terminals respectively. These measurements are typically obtained using a Phasor Measurement Unit (PMU). PMUs estimate the phase, frequency, frequency modulation and amplitude of the fundamental grid frequency (60Hz in the U.S.). The primary PMU generated measurement, however, is called a synchrophasor which is a vector representation of a sinusoidal voltage and current waveform as illustrated in Figure 3.

Several algorithms exist to compute the synchrophasor, however a majority of the algorithms utilize a recursive peak tracking implementation of the discrete Fourier transform or a similar algorithm [8]. The synchrophasor phase angle θ is measured in reference to the 'second' transition on a UTC synchronized clock within the PMU. As a result, clock offsets in the PMU clock manifest as phase error of the vector measurement [9].

The C37.118.1-2011 synchrophasor standard and its amendment [10], [11] bound the total vector error (TVE) for synchrophasors to a threshold ϵ (typically $\epsilon \leq 1\%$ under steady state conditions). TVE is the magnitude of the error vector between the true synchrophasor for a given sinusoidal waveform to the phasor measured by the PMU. The TVE bound includes all sources of error within the PMU including errors in the potential transformers and other transducers, limitations in sampling, A/D conversion and timing errors. The TVE limit is illustrated in Figure 3 by a circle with radius ϵ. Note that the maximum tolerable phase error PE is represented by tangents to the circular TVE region.

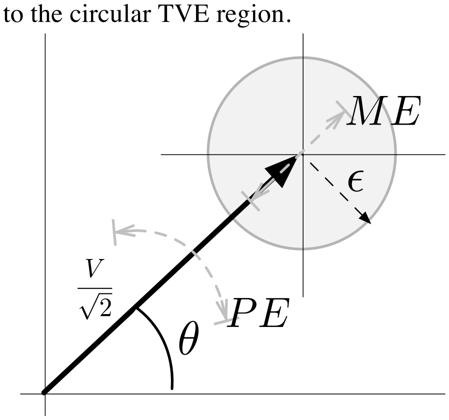

Figure 3: A synchrophasor plotted on the I/Q plane showing limits for total vector error.

Equation 3: TVE in terms of magnitude and phase error

$$TVE^2(\%) = \left\{ \left[\left(1 + \frac{ME(\%)}{100}\right) \cos(PE) - 1 \right]^2 + \left[\left(1 + \frac{ME(\%)}{100}\right) \sin(PE) \right]^2 \right\} \times 100\%$$

Transforming the TVE criterion from the I/Q plane to a real basis of magnitude and phase errors, we get the relation shown in Equation 3. Where PE and ME correspond to phase and percent magnitude errors respectively. An interesting outcome of this change of basis is that the graphical interpretation of Equation 3 is an ellipsoidal level set.

Figure 4 shows the level curves for Equation 3 at different values of ϵ. Based on this geometric interpretation, we propose that uncertainty in the system state x for the microgrid system, as measured by a PMU, may be represented by a spherical or hyper-ellipsoidal geometric error criterion. Our uncertainty model is not stochastic but rather deterministic and set based. In the following sections, we will extend this interpretation of uncertainty and generalize our uncertainty model in order to develop a non-probabilistic test for safety or correctness of the two generator power system for any realization of state uncertainty within the set.

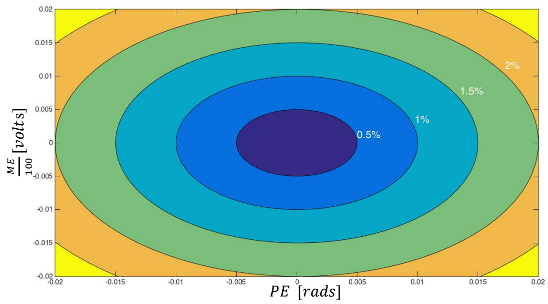

Figure 4: Contour plot showing ellipsoidal level curves corresponding to different values of ϵ

4) UNCERTAINTY FROM TIMING COMPONENTS

An important factor affecting PMU performance is its internal timing system. As highlighted in the previous section, timing errors result in errors in measurement of phase. Prior evaluations of PMU performance and uncertainty include timing errors in their analysis by simply translating the maximum tolerable measurement error to the corresponding clock offset i.e. for the $\epsilon \leq 1\%$ criterion to hold in a 60 Hz system, errors in the timing system must be ≤26.5 μs. Clearly, this is a fairly superficial treatment of timing errors. As the constraints on sensor performance are tightened and the complexity of algorithms used for CPS continually increase, there is concern in the metrology community that the dynamics associated with clock regulation and time synchronization might result in rare but unpredictable negative interactions within a CPS.

Let us re-examine PMU measurement uncertainty from the perspective of first order effects introduced by phase noise in the primary oscillator driving its sampling clock.

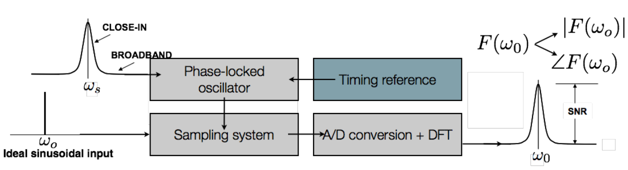

Figure 5: Schematic diagram showing measurement noise introduced through phase modulation of the sampling clock.

Assuming that the measurand is an ideal sinusoidal signal ω_0, Figure 5 illustrates the impact of phase noise in the sampling clock ω_s on the Signal-to-Noise ratio of the output signal $F(\omega_0)$ from the PMU [12]. When the sampling clock is derived from a free running oscillator its single side-band phase noise in dBc/Hz is typically a function of frequency offset from the oscillator resonant frequency. This function is available as published test data for the oscillator typically approximated to a number of regions having a slope of $1/f^x$. Figure 6 shows an example of this phase noise profile published in [13]. We assume for simplicity that the time domain jitter is dominated by "white" broadband phase noise. An assumption justified by the fact that sampling clocks in PMUs are typically phase locked oscillators. Phase locked loops significantly attenuate close-in phase noise. We can then compute the timing jitter introduced by the integrated noise power across a frequency domain of interest. Typically, a range of twice the sampling rate is adequate as shown in Figure 6 by the brown highlighted rectangular region.

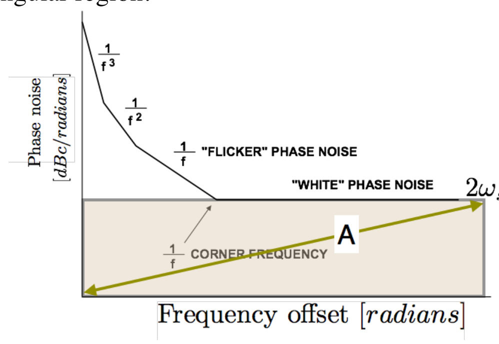

Figure 6: Oscillator phase noise profile

The root mean square timing jitter introduced by the total phase noise represented by the area labeled 'A' is given by:

$$T_{jitter} = \frac{\sqrt{2 \cdot 10^{A/10}}}{\omega_s}$$

We can now perform a change of basis in a similar fashion to the previous section to find the manifestation of this timing jitter in the output of an N-point Discrete Fourier Transform computed from discrete samples $f_n\ [n \in N]$.

First, assuming that T_{jitter} is uniformly distributed across the N sample DFT window, the standard deviation of the sampled signal in the time domain is given by:

$$U_n = \sqrt{\mathrm{E}[\alpha_n^2]} = \alpha_n \cdot T_{jitter}$$

Where α_n is the first derivative of the sampled sinusoidal (60Hz) waveform at sampling instant n.

Transforming this uncertainty to the phasor space or the I/Q plane as in Figure 3 we get the relation in Equation 4. See [14] for a more detailed presentation.

Equation 4: Uncertainty associated with sampling jitter

$$U^2_{I(\omega_0)}|T_{jitter} = \sum_{n=0}^{N-1} f_n \cos^2(\frac{\omega_0 n}{N}).U_n^2$$

$$U^2_{Q(\omega_0)}|T_{jitter} = \sum_{n=0}^{N-1} f_n \sin^2(\frac{\omega_0 n}{N}).U_n^2$$

$U^2_{I(\omega_0)}$ and $U^2_{Q(\omega_0)}$ correspond to the magnitude of uncertainty on the I and Q axes respectively. Adding these two terms we see that by the trigonometric identity $\sin^2 x + \cos^2 x = 1$ that the geometric interpretation of the cumulative uncertainty in signal magnitude and phase due to timing jitter is ellipsoidal in nature. As in Section 3 with sensor uncertainty, timing uncertainty can also be modeled using a set based hyper-ellipsoidal geometric error criterion.

4.1) Dynamics of timing components

Our analysis of timing uncertainty so far has focused on jitter and phase noise as ergodic parameters. There are also deterministic dynamics at play in the timing system that are seldom included when evaluating the correctness of CPS. For example, consider the dynamics of jitter mitigation and clock synchronization introduced into the sampling subsystem in a PMU. In the following analysis we focus on the dynamics of a three state charge-pump phase locked loop (3PD-CP-PLL) in conjunction with a voltage-controlled crystal oscillator (VCXO). This type of PLL is popular in embedded analog to digital converters and is unique in that the output of its phase detector is a current that is 'pumped' in and out of a loop-filter and is able to serve as a frequency detector as well. The reader is directed to [15]–[17] for more detailed discussion on PLL design illustrated in Figure 7.

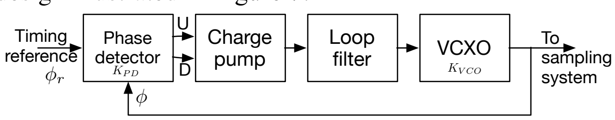

Figure 7: Block diagram of 3PD-CP-PLL driving the sampling system

The linearized closed loop dynamics associated with phase ϕ and frequency modulation ω due to the PLL can be described by the following differential equation:

$$\begin{bmatrix} \dot{\phi}(t) \\ \dot{\omega}(t) \end{bmatrix} = \begin{bmatrix} 0 & 1 \\ -2K_{PD}K_{VCO}\cdot\omega_s & -2\omega_s \end{bmatrix} \begin{bmatrix} \phi(t) \\ \omega(t) \end{bmatrix} + \begin{bmatrix} 0 \\ 2K_{PD}K_{VCO}\cdot\omega_s \end{bmatrix}$$

The phase detector has three discrete operating modes (phase lead, phase lock and phase lag) that can be represented by the finite state machine in Figure 8. Note that the three state phase detector in conjunction with the linearized PLL dynamic equation produces a hybrid automata of the form described in Section 2.

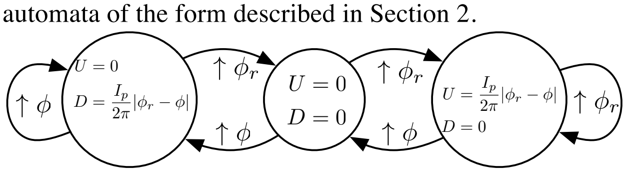

Figure 8: Hybrid system model of a three state phase detector.

The core challenge we address in our work is the propagation of uncertainty expressed in Equation 3 and Equation 4 through the dynamics shown in Figure 2 and Figure 8. In a larger sense, we are interested in a computationally feasible strategy to evaluate the impact of uncertainty originating from subsystems such as the timing system or the sampling system on the performance of a CPS. Our approach is a treatment of uncertainty using the same compositional primitives used to effectively compose a CPS from sub-systems. In the following section we will present one strategy to achieve this goal by exploiting the spherical and ellipsoidal fitting of geometric error criterion (such as TVE or Timing jitter) in $\mathbb{R}^n$.

5) REACHABILITY ANALYSIS

We treat uncertainty propagation as a dual to the problem of reachability of hybrid dynamic systems i.e., reach of a set of uncertain states represents a measure of correctness. In contrast to Monte-Carlo strategies of exploring the uncertainty space that are limited in scale to a finite number of simulated trajectories, we use a simplification of the uncertainty space represented as a convex set bounded by the functions in Equation 3 and Equation 4. Extending the observation that our convex uncertainty sets can be approximated by a family of hyper-ellipsoids $\mathcal{E}(q, Q) = \{x | \langle x - q, Q^{-1}(x - q)\rangle \le 1\} [q \in \mathbb{R}^n, Q \in \mathbb{R}^{n \times n}]$ we use the results in [11] and [12] to propagate these ellipsoids through hybrid automata with small signal linear dynamics $\dot{x} \subseteq Ax + Bu$: Using the linear transformation $A[\mathcal{E}(q, Q)] + b = \mathcal{E}(Aq + b, AQA^T)$.

The guards of the discrete transition $X' \to X$ (recall the notation for the hybrid automaton H) are usually represented as linear inequalities. If the geometric interpretation of these inequalities is a half space $S = \{x | \langle b, x\rangle \ge \alpha\}$ then the ellipse $\mathcal{E}\big(q + (p), Q + (p)\big)$ is an approximation of $\mathcal{E}(q, Q) \cap S$ at any point $p \in \left[0, \frac{\alpha' + 1}{2}\right)$.

The geometric union of ellipsoids can also be estimated by an approximating ellipse $\mathcal{E}\big(q_1 + q_2, Q(\beta)\big) \subset \mathcal{E}(q_1, Q_1) \cup \mathcal{E}(q_2, Q_2)$ s.t. $Q(\beta) = (1 + \beta^{-1})Q_1 + (1 + \beta)Q_2 \; \forall \beta > 0$.

Using these geometric operations, we are able to analytically determine the correctness of hybrid systems for any realization of the uncertainty in a given set. As a result, correctness as evaluated using this approach is deterministic. In hybrid systems with a large number of interacting components, this deterministic approach consumes significantly less memory than comparable probabilistic approaches since each ellipse is stored as a tuple and every interaction between subsystems manifests as an intersection of ellipses which in turn is approximated as an ellipse. In comparison interacting dissimilar probability distributions result in very large sets of posterior probabilities.

Geometric operations for the intersection, union, linear transformation and geometric sum of convex sets can be performed very efficiently. As noted in [18], the complexity of the reachability analysis using ellipsoidal approximations is polynomial in time and quadratic in dimension. While a more detailed presentation of verification guarantees for our ellipsoidal approximations are beyond the scope of this paper, we would like to highlight our approach as it applies to the CPS example in Section 2.1. First, the ability to efficiently detect intersections between ellipses and half spaces gives us a tool to test the hybrid system for violations such as the limit threshold on circuit breaker Q_1. Second, the geometric union of ellipses gives us the ability to compose multiple sources of uncertainty as in the uncertainty originating from PMUs expressed as TVE and the sampling jitter introduced by the timing system. Algorithms used to detect intersections and unions are either closed form, or guaranteed to converge to the global optimum in a finite number of iterations and they work without restriction in spaces of generic dimension. Lastly, the dynamics of the generators, the PLL system and the electrical network constraints are implemented as linear transformations on uncertainty ellipses. As described in [20], parameter uncertainty in dynamic models may also be expressed as unknown but bounded sets and so may be considered using our approach.

6) CONCLUSIONS AND FUTURE EXTENSIONS

As a preliminary evaluation of our approach, we considered two operating conditions for our CPS example. In the first case, an uncertainty set bounded by $\mathcal{E}\left\{\begin{bmatrix}0\\0\end{bmatrix},\begin{bmatrix}1 & 0\\0 & 0.5\end{bmatrix}\right\}$ was applied to the hybrid system comprising the charge pump PLL and the two generator network. Both systems are asymptotically stable in their primary operating modes and as a result $|Q|$ remains bounded as the reach set is propagated through the system dynamics. Figure 9 illustrates the evolution of reach set over ten simulated seconds constructing a 'reach tube'.

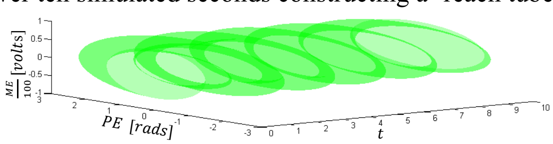

Figure 9: Reach tube showing stable evolution of phase and magnitude variation when the initial uncertainty set does not trip the circuit breaker.

Repeating the analysis for a case when the reach set intersects the half space facet representing a circuit breaker tripping event, we see that the same uncertainty set results in unbounded expansion of the reach set. Clearly not all trajectories are unstable within the set but the analysis does show that a sequence of dynamic transitions are possible that might drive the system to an unstable operating state. The phase tracking system, therefore, is no longer 'correct'.

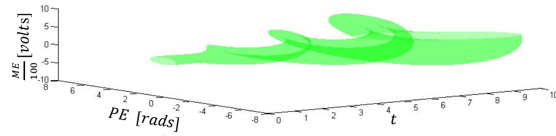

Figure 10: Reach tube showing an unstable evolution of phase and magnitude when the uncertainty set erroneously triggers a tripping event.

The analysis presented here is fairly simple in order to introduce our approach and to present its value to evaluating the correctness of hybrid dynamic systems; particularly in relation to the impact of timing uncertainty on large interconnected CPS. Our research continues to focus on this reachability approach for compositions of interconnected subsystems with a large number of set intersections. Our upcoming work includes simulations using real data for timing uncertainties and model parameters.

REFERENCES

[1] R. Baheti and H. Gill, "Cyber-physical systems," *impact Control Technol.*, vol. 12, pp. 161–166, 2011.

[2] A. D. Stoyenko, *Constructing predictable real time systems*, vol. 146. Springer Science & Business Media, 2012.

[3] E. Asarin, O. Maler, and A. Pnueli, "Reachability analysis of dynamical systems having piecewise-constant derivatives," *Theor. Comput. Sci.*, vol. 138, no. 1, pp. 35–65, Feb. 1995.

[4] J.-F. Raskin, "An introduction to hybrid automata," in *Handbook of networked and embedded control systems*, Boston: Birkhäuser, 2005, pp. 491–517.

[5] M. Prodanovic and T. C. Green, "High-Quality Power Generation Through Distributed Control of a Power Park Microgrid," *IEEE Trans. Ind. Electron.*, 2006.

[6] F. Pasqualetti, A. Bicchi, and F. Bullo, "A graph-theoretical characterization of power network vulnerabilities," in *American Control Conference*, 2011.

[7] J. Glover, M. Sarma, and T. Overbye, *Power Systems Analysis and Design*. CL-Engineering, 2007.

[8] A. G. Phadke and B. Kasztenny, "Synchronized phasor and frequency measurement under transient conditions," *Power Deliv. IEEE Trans.*,

vol. 24, no. 1, pp. 89–95, 2009.

[9] K. Narendra, D. Gurusinghe, and A. Rajapakse, "Dynamic Performance Evaluation and Testing of Phasor Measurement Unit (PMU) as per IEEE C37. 118.1 Standard," *Int. Prot. Test. Users Gr.*

[10] P. S. R. Committee, "IEEE Standards for Synchrophasor Measurements for Power Systems-IEEE Std C37. 118.1-2011," New York, 2011.

[11] K. E. Martin, "Synchrophasor Measurements Under the IEEE Standard C37.118.1-2011 With Amendment C37.118.1a," *Power Deliv. IEEE Trans.*, vol. 30, no. 3, pp. 1514–1522, Jun. 2015.

[12] T. C. Weigandt, B. Kim, and P. R. Gray, "Analysis of timing jitter in CMOS ring oscillators," in *Circuits and Systems, 1994. ISCAS'94., 1994 IEEE International Symposium on*, 1994, vol. 4, pp. 27–30.

[13] W. Kester, "Converting Oscillator Phase Noise to Time Jitter," 2009.

[14] G. Betta, C. Liguori, and A. Pietrosanto, "Propagation of uncertainty in a discrete Fourier transform algorithm," *Measurement*, vol. 27, pp. 231–239, 2000.

[15] R. E. Best, *Phase locked loops*. McGraw-Hill Professional, 2007.

[16] C. A. Sharpe, "A 3-state phase detector can improve your next PLL design," *EDN Mag.*, vol. 9, pp. 55–59, 1976.

[17] M. Van Paemel, "Analysis of a charge-pump PLL: a new model," *IEEE Trans. Commun.*, vol. 42, no. 7, pp. 2490–2498, 1994.

[18] O. Botchkarev and S. Tripakis, "Verification of hybrid systems with linear differential inclusions using ellipsoidal approximations," *Hybrid Syst. Comput. Control*, pp. 73–88, 2000.

[19] R. Lorenz and S. Boyd, "An ellipsoidal approximation to the Hadamard product of ellipsoids," *IEEE Conference on Acoustics, Speech, and Signal Processing*. pp. 1193–1196, 2002.

[20] M. Milanese and A. Vicino, "Optimal estimation theory for dynamic systems with set membership uncertainty: an overview," in *Bounding Approaches to System Identification*, Springer, 1996, pp. 5–27.